Tetracarboxylic acid cobalt phthalocyanine SAM on gold: Potential applications as amperometric sensor for H_2O_2 and fabrication of glucose biosensor

Philani N. Mashazi, Kenneth I. Ozoemena, and Tebello Nyokong

Abstract

This report describes the applications of cobalt tetracarboxylic acid phthalocyanine (CoTCAPc) self-assembled monolayer (SAM) immobilized onto a preformed 2-mercaptoethanol (Au-ME) SAM on gold surface (Au-ME-CoTCAPc SAM) as a potential amperometric sensor for the detection of hydrogen peroxide (H_2O_2) at neutral pH conditions. The Au-ME-CoTCAPc SAM sensor showed a very fast amperometric response time of approximately 1 s, good linearity at the studied concentration range of up to 5 μM with a coefficient $R^2 = 0.993$ and a detection limit of 0.4 μM oxidatively. Also reductively, the sensor exhibited a very fast amperometric response time (~1 s), linearity up to 5 μM with a coefficient $R^2 = 0.986$ and a detection limit of 0.2 μM. The cobalt tetracarboxylic acid phthalocyanine self-assembled monolayer was then evaluated as a mediator for glucose oxidase (GOx)-based biosensor. The GOx (enzyme) was immobilized covalently onto Au-ME-CoTCAPc SAM using coupling agents: *N*-ethyl-*N*(3-dimethylaminopropyl) carbodiimide (EDC) and *N*-hydroxy succinimide (NHS), and the results demonstrated a good catalytic behavior. Kinetic parameters associated with the enzymatic and mediator reactions were estimated using electrochemical versions of Lineweaver–Burk and Hanes equation, and the stability of the sensor was tested. The biosensor (Au-ME-CoTCAPc-GOx SAM) electrode showed good sensitivity (7.5 nA/mM) with a good detection limit of 8.4 μM at 3σ, smaller Michaelis–Menten constant (4.8 mM from Hanes plot) and very fast response time of approximately 5 s.

1. Introduction

The development of the reliable, rapid and simple methods for the detection and monitoring of hydrogen peroxide (H_2O_2) is important. Methods for the determination of H_2O_2 include spectrometry [1], chromatography [2] and [3], chemilumiscence [4] and [5], titrimetry [6] and electrochemistry [7], [8], [9], [10], [11], [12], [13], [14] and [15]. Amongst these methods, electrochemical methods are preferred over others because of their simplicity, low detection limits, fast response time and relatively low costs. Electrochemical determination of H_2O_2 has been studied in many laboratories using porphyrin or phthalocyanine modified electrodes [7], [11], [12], [13], [15], [16], [17], [18] and [19], including cobalt phthalocyanine [12], [17] and [18], cobalt tetraruthenated porphyrin [13], polymerized cobalt tetrakis(*o*-aminophenyl) porphyrin [19] and in our laboratory we have recently reported on the determination of H_2O_2 using a pentamer consisting of four cobalt tetraphenyl porphyrins attached to a cobalt phthalocyanine, CoPc-$(CoTPP)_4$, as an electrode modifier [15]. Electrocatalysis of H_2O_2 under physiological pH conditions is of importance in many biomedical and environmental studies. The reported electrodes have been mostly used in alkaline pH [13], [18] and [19], which is inappropriate for enzyme electrode. Also some of these electrodes modified by cobalt phthalocyanine have been mostly based on the oxidation of H_2O_2 [12], [15] and [18] with the limited reports on the reduction of H_2O_2 which occurs at negative potentials [16]. Therefore, this work reports the

construction of an amperometric sensor based on the self-assembled monolayer of cobalt tetracarboxylic acid phthalocyanine (CoTCAPc) immobilized onto gold electrode for the oxidative and reductive detection of H_2O_2 under physiological pH. We also report on the fabrication of glucose oxidase (GOx) enzyme on gold electrode modified with an electrocatalyst CoTCAPc. Enzyme electrodes are also important as they are selective and specific towards the analytes of interest. In particular glucose oxidase enzyme has attracted more attention since it is highly specific, stable and practically applicable enzyme for the detection of β-D-glucose. Glucose oxidase sensors are very important due to their usefulness in diagnosis of diabetes. The first step of the formation of CoTCAPc SAM is the immobilization of the cobalt tetracarboxylic acid chloride phthalocyanine (CoTCAClPc), following the coordination of one carboxylic acid chloride bond to 2-mercaptoethanol (2-ME), the exposed acid chlorides groups are hydrolyzed to carboxylic acid, giving cobalt carboxylic acid phthalocyanine SAM (CoTCAPc SAM).

The mechanism of action of glucose oxidase biosensors is based on monitoring the consumption of O_2 or the production of H_2O_2, with the latter being more convenient. However, the amperometric determination of hydrogen peroxide requires high anodic potentials and this has lead to the introduction of mediators [2], [20], [21], [22], [23], [24], [25], [26], [27], [28] and [29] which are used to facilitate transfer of electrons between the redox centre of the enzyme and the electrode surface, the mechanism is shown in Scheme 1. The enzyme (due to its specificity) oxidizes β-D-glucose leading to the generation of H_2O_2, which diffuses to the CoTCAPc layer immobilized on gold electrode, and gets oxidized. Metallophthalocyanines (MPc), particularly cobalt phthalocyanine [2], [18], [25], [26], [27] and [28] have been found to be biocompatible with glucose oxidase enzyme [17], [18] and [24]. There have been limited reports of MPc complexes immobilized on the gold surface, due to the difficulty in synthesizing sulfur containing phthalocyanine complexes. However, we have recently reported on the easier technique of immobilizing tetra-acid chloride cobalt phthalocyanine to form a self-assembled monolayer (SAM) on the preformed 2-mercaptoethanol onto gold electrode [30], hence avoiding the synthesis of thiol-substituted phthalocyanine. This method offers various advantages such as the ease of formation of stable self-assembled monolayer of CoTCAPc. The interesting electrochemical properties exhibited by this type of MPc-SAM have prompted us to further investigate its applications as an amperometric sensor for H_2O_2 and also possibility of attaching glucose oxidase enzyme to the CoTCAPc via the covalent attachment using *N*-ethyl-*N*(3-dimethylaminopropyl) carbodiimide hydrochloride (EDC) and *N*-hydroxy succinimide (NHS) coupling agents.

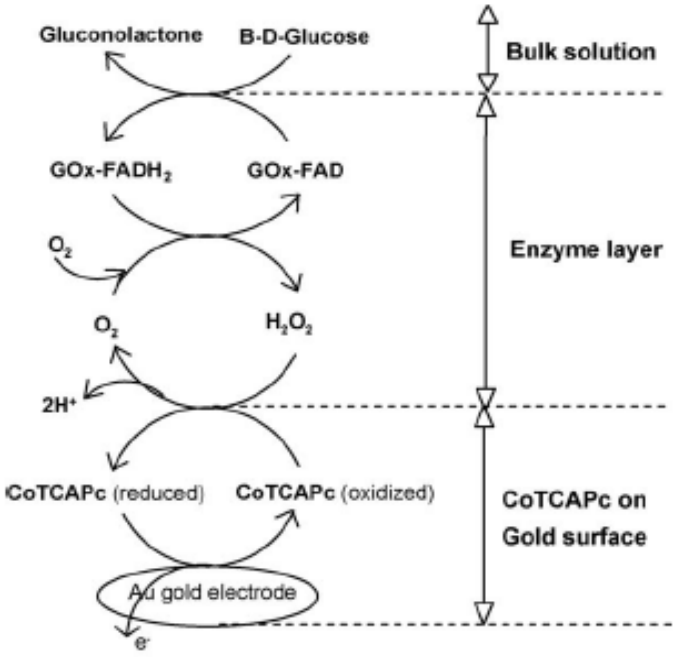

Scheme 1. Schematic representation of enzyme reaction with CoTCAPc-SAM as an electron mediator.

2. Experimental details

2.1. Materials used

Glucose oxidase (GOx, EC 1.1.3.4, from *Aspergillus niger*, Type VII), *N*-ethyl-*N*(3-dimethylaminopropyl) carbodiimide hydrochloride (EDC), *N*-hydroxy succinimide (NHS), 2-mercaptoethanol (ME), dimethylformamide (DMF), ferricyanide ($K_3Fe(CN)_6$), ferrocyaninde ($K_4Fe(CN)_6$), potassium chloride (KCl), 30% hydrogen peroxide (H_2O_2) and glucose for laboratory use were purchased from Sigma–Aldrich. Absolute ethanol (EtOH) was purchased from SAARCHEM and used as received. All other reagents were of analytical grade, and all chemical solutions were prepared using ultra pure water obtained from a Milli-Q Water System (Millipore Corp., Bedford, MA, USA). Clinical glucose powder (Alpha®, South Africa) was bought from a local pharmacy shop.

Phosphate-buffered saline (PBS) solution (0.01 M, pH 7.4) was prepared following the reported method [31] using appropriate amounts of K_2HPO_4, KH_2PO_4 and chloride salts, dissolved in ultra pure water. Ferricyanide ($K_3Fe(CN)_6$, 1 mM) solution was prepared using pH 7.4 PBS solution. For the activation of carboxylic acid group, the PBS (pH 7.4) solution containing 2 mM NHS and 5 mM EDC was used. Glucose oxidase enzyme solution (150 mg/ml) for immobilization was prepared using pH 7.4 PBS solution and the enzyme was immobilized at a low temperature (4 °C). H_2O_2 solutions were deaerated before each experiment to eliminate the possible interference of O_2 reduction at negative potentials. The synthesis of cobalt(II)-2,9,16,23-tetracarboxylic acid chloride phthalocyanine (CoTCAClPc) via the cobalt tetracarboxylic acid phthalocyanine (CoTCAPc) has been reported [30].

2.2. Electrochemical apparatus and methods

Electrochemical experiments, cyclic voltammetry and chronoamperometry were performed using Bio-Analytical Systems (BAS) model 100 B/W electrochemical workstation. A conventional three-electrode system was used. The working electrode was either a bare gold (0.8 mm radius) or gold modified with the SAM of mercaptoethanol (represented as Au-ME) or CoTCAPc (represented as Au-ME-CoTCAPc) or with enzyme (Au-ME-CoTCAPc-GOx). Silver–silver chloride (Ag|AgCl) and platinum wire were used as pseudo-reference and counter electrodes, respectively. The potential response of Ag|AgCl pseudo-reference in aqueous conditions was less than the Ag|AgCl (3 M KCl) by 0.015 ± 0.03 V. A WTW® pH meter was used for pH measurements. Electrochemical impedance spectroscopy experiments were recorded in the frequency range between 10 kHz to 100 mHz at a formal potential of 150 mV and with an amplitude 5 mV rms sinusoidal modulation. An AUTOLAB PGSTAT30 potentiostat/galvanostat, connected to a computer and controlled by GPES and FRA software, was used for acquisition and analysis of the impedance data. The impedance measurements were performed using the prepared solution of 1 mM of $K_4Fe(CN)_6$ and 1 mM $K_3Fe(CN)_6$ (1:1) mixture in 0.1 M KCl solution. The impedance spectra were plotted in the form of a complex plane diagrams (Nyquist plot). All experiments were performed at 25 ± 1 °C. UV–vis spectra were recorded on a Varian 500 UV–vis/NIR spectrophotometer. Infrared (IR) spectra were recorded on a Fourier Transform Infrared (FTIR) spectrophotometer. The frequency change leading to the estimation of mass gain for the surface-confined GOx was recorded using Quartz Crystal Microbalance with Dissipation (QCM-D) equipment purchased from Q-Sense (Sweden).

2.3. Preparation of glucose oxidase enzyme electrode (Scheme 2)

Prior to the immobilization of the enzyme onto the surface of the gold electrode, the surface was cleaned using the established procedures [32] and [33]. Briefly, the gold electrode was first polished using an aqueous slurries of alumina (<10 μm) on a SiC-emery paper (type 2400 grit), and then to a mirror finish on a Buehler felt pad. The electrode was then placed in ethanol and subjected to ultrasonic vibration to remove residual alumina particles that might be trapped at the surface. Finally the electrode was etched for about 2 min in a “Piranha” solution {3:1 (v/v) 30% hydrogen peroxide (H_2O_2) and concentrated sulfuric acid (H_2SO_4)} and then rinsed with copious amounts of ultra pure Millipore water followed by ethanol. The cleanliness of bare gold electrode surface was finally established by placing it in 0.5 M H_2SO_4 and scanning the potential between −0.5 and 1.0 V (versus Ag|AgCl) at a scan rate of 50 mV/s until a reproducible scan was obtained. Following this pre-treatment the electrode was rinsed with absolute ethanol and immediately placed into a nitrogen saturated absolute ethanol solution of 3 mM 2-mercaptoethanol at ambient temperature for 10–14 h. The 2-mercaptoethanol modified gold electrode (Au-ME SAM) was thoroughly rinsed with absolute ethanol before reacting with CoTCAClPc, this step is important because it removes the physically adsorbed 2-mercaptoethanol molecules. The coordination reaction between CoTCAClPc and Au-ME SAM, step 1 (ii) in Scheme 2, was performed by immersing the 2-mercaptoethanol modified electrode into a dry dimethylformamide (DMF) solution of CoTCAClPc (0.2 mM) for 24 h. Upon removal from the deposition solution, the electrode was rinsed with dry DMF to remove the unreacted CoTCAClPc. The unreacted acid chloride groups of the

CoTCAClPc SAM undergo hydrolysis (in pH 4 phosphate buffer) to carboxylic acid groups to form Au-ME-CoTCAPc SAM, step 2. The Au-ME-CoTCAPc SAM electrode was then rinsed with pH 7.4 PBS solution and immediately immersed into the solution containing 2 mM EDC and 5 mM NHS [34] for 3 h to convert the carboxylic acid into reactive intermediates (Scheme 2, step 3) which are susceptible to attack by amine groups from the enzyme (GOx). The activated electrode was then washed with pH 7.4 PBS solution and immediately immersed in the pH 7.4 PBS solution containing 150 mg/ml of GOx (Scheme 2, step 4) for 3 h at 4 °C to allow for covalent attachment of the enzyme to CoTCAPc forming a SAM on gold electrode (represented as Au-ME-CoTCAPc-GOx SAM). To confirm the coordination of the terminal OH^- group of the mercaptoethanol with the CoTCAClPc, the product of the reaction between the complexes was then dried and IR spectra recorded. IR[(KBr) V_{max} (cm^{-1})]: 1699 (C═O stretch), 1141 (C—O—C stretch). The hydrolysis of the CoTCAClPc was also checked by first exposing CoTCAClPc in pH 4 phosphate buffer solution, then filtered, dried and the IR spectrum recorded. IR[(KBr) V_{max} (cm^{-1})]: 3422 (OH), 1699 (C═O stretch). The amount of the surface-confined GOx was estimated using the QCM-D equipment, where the 15 MHz or first overtone was used to estimate the mass gain. The gold coated crystal with an area of 1.13 cm^2 was used in QCM-D to estimate the amount of GOx on the surface. The frequency change of about 50 Hz was observed and the mass gain was estimated using the built-in QTools software with built-in Sauerbrey relationship.

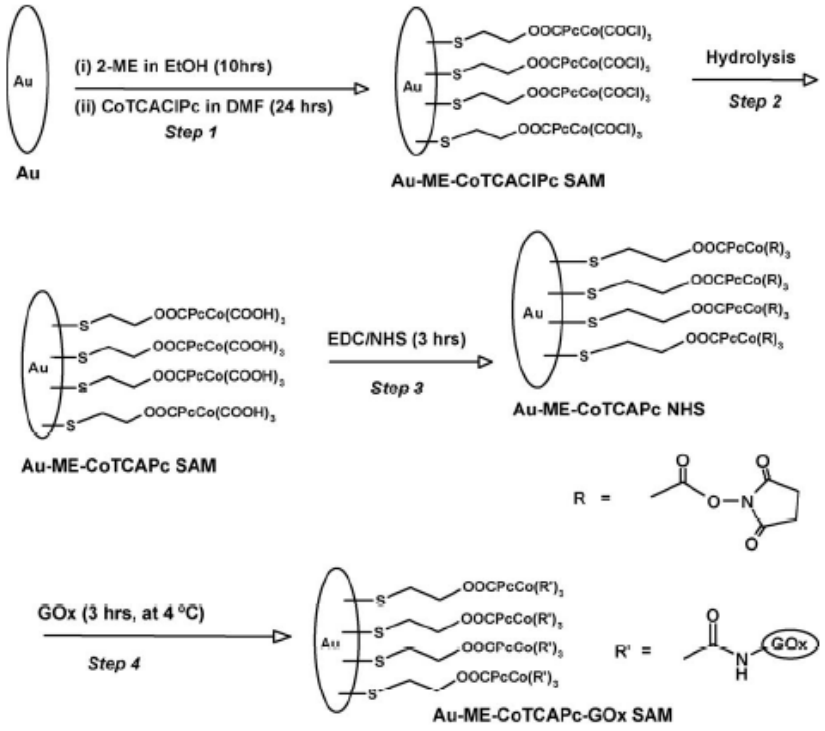

Scheme 2. Schematic representation showing the covalent attachment of glucose oxidase enzyme electrode (Au-ME-CoTCAPc-GOx SAM) onto gold electrode, via activated acid groups of CoTCAPc (Au-ME-CoTCAPc NHS SAM).

3. Results and discussion

3.1. Formation of Au-ME-CoTCAPc-GOx-SAM

CoTCAClPc was first immobilized covalently onto a preformed mercaptoethanol gold electrode following the method recently reported [30]. The acid chloride groups on the CoTCAClPc were allowed to undergo hydrolysis in the phosphate buffer solution (pH 4.0) to form acid groups, CoTCAPc (Scheme 2, step 2). The possible coordination of OH group to the acid chloride group of CoTCAClPc was evident from IR spectroscopic bands at 1699 and 1141 cm^{-1} corresponding to (C═O stretch) and (C—O—C stretch), respectively. Also, we observed a broad OH band at 3422 cm^{-1} with a shift of the C═O band of CoTCAClPc from 1735 to 1699 cm^{-1}, confirming the hydrolysis of CoTCAClPc to CoTCAPc. The enzyme may be immobilized onto Au-ME-CoTCAPc following the method reported by Gooding et al. [34], [35] and [36]. This will allows the formation of the covalent bond between the exposed carboxylic acid groups of the Au-ME-CoTCAPc SAM and the amino groups of the GOx enzyme. The reaction between the amino groups of the enzyme and the acid group of the Au-ME-CoTCAPc monolayer did not occur without coupling agents, as was evident by the lack of changes in cyclic voltammograms (CVs). Thus, EDC and NHS, were used as coupling agents which catalyze the formation of amide bond between the carboxylic acid and amine groups as shown in Scheme 2, step 3. The activated carboxylic acid groups form reactive intermediates which are susceptible to attack by amines. Following this method we achieved the covalent attachment of glucose oxidase as shown in Scheme 2 (step 4) forming Au-ME-CoTCAPc-GOx SAM. In this GOx enzyme immobilized electrode, Au-ME-CoTCAPc SAM will act as an electron mediator between the redox enzyme and electrode surface. Jiang et al. [37] have estimated that using the mixture of EDC and NHS, about 60% of carboxylic acid groups are NHS-activated, 30% EDC-activated leaving only 10% not activated.

3.2. Surface electrochemistry of CoPc SAM modified gold electrode

Surface roughness calculations are important in characterization of an unmodified gold electrode as they give the clear indication of the surface morphology. The surface morphology is known to affect the properties of the self-assembled monolayer, such as defect densities [38]. An ideally smooth plane of gold electrode is expected to give the most highly ordered and regularly packed monolayer [39]. The surface roughness factor is also important in the determination of the real surface area of the electrode, as by definition the surface roughness factor is the ratio of the real surface area to the geometric area [40] and [41]. In this work, the surface roughness of the gold electrode was measured using the conventional methodology [39] and [42], using $K_3Fe(CN)_6$ solution and Randles–Sevcik Eq. (1):

$$I_{pa}=(2.69\times10^5)n^{3/2}AD^{1/2}Cv^{1/2} \quad (1)$$

where n is the number of electrons involved (n = 1) in the $Fe(CN)_6^{3-/4-}$ system, A the geometric surface area of the electrode (0.0201 cm^2), C the bulk concentration of $Fe(CN)_6^{3-}$ (5 mM), $D = 7.6 \times 10^{-6}$ the diffusion coefficient of $Fe(CN)_6^{3-}$ (cm^2/s) [43], and v is the scan rate solution (0.050 V/s). The experimental measurements, Fig. 1(i), gave $I_{pa} = 2.780 \times 10^{-6}$ A, leading to a real surface are of 0.0335 cm^{-2} and the surface roughness factor of 1.67. The calculated roughness factor was found to be within the reported values for the gold electrode [40], [44] and [45].

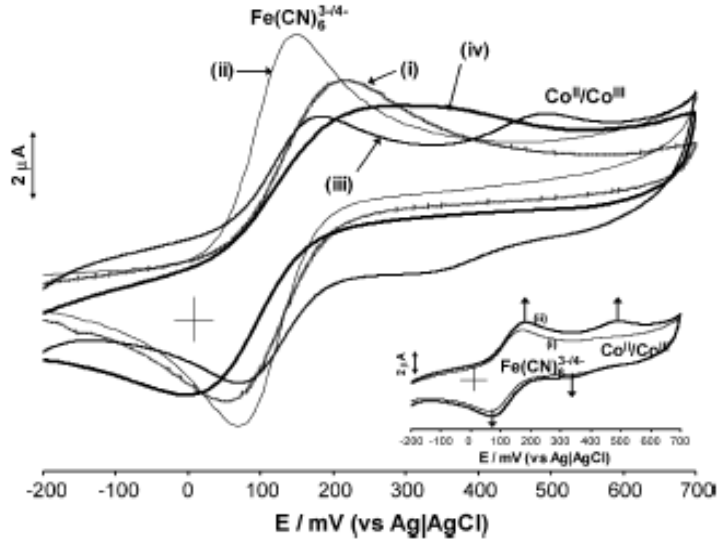

Fig. 1. Cyclic voltammograms 5 mM $K_3Fe(CN)_6$ in 0.01 M PBS (pH 7.4) on: (i) bare gold electrode, (ii) Au-ME SAM, (iii) Au-ME-CoTCAPc SAM after conditioning and (iv) Au-ME-CoTCAPc-GOx. Insert: cyclic voltammograms showing continuous cycling CoTCAPc-SAM (Au-ME-CoTCAPc SAM) in 5 mM $K_3Fe(CN)_6$ in 0.01 M PBS (pH 7.4) solution. Arrows show the trend of peak current shift.

The surface coverages of the ME and CoTCAPc SAM on gold were reported previously [30] as 5.8×10^{-10} and 4.6×10^{-10} mol/cm^2, respectively, using the geometric area (0.0201 cm^2) of the electrode. Using real surface area of 0.0335 cm^2, the surface coverages of ME and CoTCAPc SAM on gold were recalculated and were estimated to be 3.48×10^{-10} and 2.76×10^{-10} mol/cm^2, respectively. The estimated surface coverage of an immobilized CoTCAPc of 2.76×10^{-10} mol/cm^2 is about three times that of a molecule lying flat on the surface (1×10^{-10} mol/cm^2) [46] and [47], confirming the expected perpendicular orientation for CoTCAClPc SAM. From the QCM-D experiments, the estimated mass of GOx on the Au-ME-CoTCAPc-GOx SAM electrode was 1.10 μg.

Electrochemical methods, especially cyclic voltammetric methods, are known to provide an excellent insight into the structure of an electroactive film adsorbed onto a surface of the electrode. The electrochemical characterization of the modified electrodes were performed using the cyclic voltammetric experiments in the presence of 5 mM $K_3Fe(CN)_6$ in PBS (pH 7.4) solution. Fig. 1 shows a typical cyclic voltammograms with redox peaks due to $Fe(CN)_6^{3-/4-}$ ($\sim$100 mV) for bare gold (i), Au-ME SAM (ii), Au-ME-CoTCAPc SAM (iii) and Au-ME-CoTCAPc-GOx SAM (iv). The redox couple due Co^{III}/Co^{II}, Fig. 1(iii) was observed at $\sim$400 mV for Au-ME-CoTCAPc SAM, it was not observed in Au-ME SAM Fig. 1(ii), and it disappeared after immobilization of the GOx enzyme in Fig. 1(iv). The disappearance of the redox couple (Co^{III}/Co^{II}) could be attributed to the CoTCAPc embedded under the enzyme layer. However, it can be noted from the cyclic voltammograms that the $Fe(CN)_6^{3-/4-}$ peak at $\sim$100 mV was clearly present even after the electrode was coated with ME (Au-ME SAM, Fig. 1(ii)), CoTCAPc (Au-ME-CoTCAPc SAM, Fig. 1(iii)) and GOx (Au-ME-CoTCAPc-GOx SAM, Fig. 1(iv)). A decrease in peak separation (ΔE_p) upon modifying with 2-mercaptoethanol and the catalyst was observed compared to the bare electrode, and it increased upon modifying with enzyme

following the trend: ΔE_p (Au-ME-CoTCAPc-GOx > Au > Au-ME-CoTCAPc > ME), and the ΔE_p values (289 > 166 > 124 > 84 mV) respectively. The fact that $Fe(CN)_6^{3-/4-}$ peak (≈100 mV) is observed on modified gold electrode could be attributed to the fact that $Fe(CN)_6^{3-/4-}$ is a fast electron transfer species, also that the SAM formed is not pinhole free, i.e. solution ion can still penetrate to the surface of the electrode. The decrease in peak separation (ΔE) on Au-ME-CoTCAPc SAM and Au-ME SAM shows that the surface is catalytic. Fig. 1(insert) shows a cyclic voltammograms for Au-ME-CoTCAPc SAM on conditioning, redox peaks gradually grew with the cycle number and stabilized after the sixth cycle. It was interesting to notice that this behavior was also noticed in literature [21] and has been attributed to the conducting film being formed on the surface of the electrode.

3.3. Impedance analysis in the presence of $Fe(CN)_6^{3-/4-}$

Impedance spectroscopy in the presence of the redox probes, like $Fe(CN)_6^{3-/4-}$, may used to study the blocking behavior of SAMs and a direct measure of the defectiveness associated with the blocking films. The redox probing species $\{Fe(CN)_6^{3-/4-}\}$ will react at the pinholes/defects [48]. The modification of gold electrode with CoTCAPc (Au-ME-CoTCAPc SAM) and enzyme (Au-ME-CoTCAPc-GOx SAM) was followed by impedance measurements. Fig. 2 shows the Nyquist plot of the (i) bare gold electrode, (ii) Au-ME SAM, (iii) Au-ME-CoTCAPc SAM and (iv) Au-ME-CoTCAPc-GOx SAM, in the presence of $Fe(CN)_6^{3-/4-}$ solution. The high frequency region of the Nyquist plot (Fig. 2) shows a semicircle related to the redox probe $Fe(CN)_6^{3-/4-}$, followed by a Warburg line in the low frequency region which corresponds to the diffusion step of the overall process. As was evident from Fig. 1, the Au-ME-CoTCAPc SAM did not block the $Fe(CN)_6^{3-/4-}$ redox peak instead it facilitated the electron transfer as was evident by the decrease in peak separation. However, the peak separation increased upon immobilizing the enzyme which could be attributed to the blocking capability of the enzyme towards $Fe(CN)_6^{3-/4-}$ redox peak. We also observed the decrease in the semicircle at the high frequency region from bare electrode, Fig. 2(i), compared to the modified gold electrode by CoTCAPc Fig. 2(iii) and an increase in semicircle upon modifying with the enzyme, Fig. 2(iv). Fig. 2(ii) which is due to Au-ME SAM exhibited a straight line without detectable semicircle at high frequencies. The fact that the semicircle for CoTCAPc modified electrode is smaller than for bare electrode, may also suggests that this molecule catalyses the redox process.

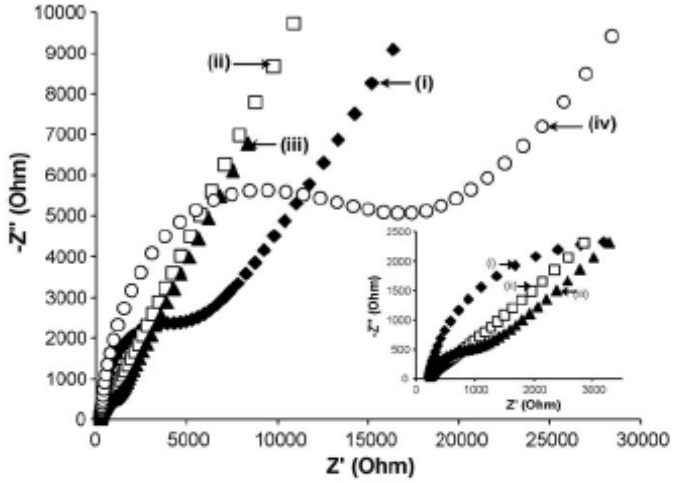

Fig. 2. Nyquist plot ($-Z''$ vs. Z') obtained from impedance measurements in the presence of 1 mM $Fe(CN)_6^{-3/-4}$ (1:1) mixture in 0.1 KCl solution for (i) bare gold electrode, (ii) Au-ME SAM, (iii) Au-ME-CoTCAPc SAM and (iv) Au-ME-CoTCAPc-GOx SAM. Insert: enlarged high frequency region for the Nyquist plot of (i) bare gold electrode, (ii) Au-ME SAM and (iii) Au-ME-CoTCAPc SAM.

At high frequency region of the impedance plot, where the electrode reaction is kinetically controlled, the charge-transfer resistance (R_{CT}) is expected to increase or decrease due to inhibition or facilitation of the electron transfer by the monolayer on the electrode [49] and [50]. The analysis of the plot in Fig. 2 shows that the charge-transfer resistance (R_{CT}) decreased from 5991 Ω (for the bare gold electrode) to 1284 Ω (for Au-ME-CoTCAPc SAM) and increased upon modifying with GOx enzyme to 15969 Ω (for Au-ME-CoTCAPc-GOx SAM). The R_{CT} for Au-ME SAM could not be integrated as the Nyquist plot showed a straight line even at high frequencies. Fig. 2 (insert) shows the enlarged high frequency region of (i) bare gold, (ii) Au-ME SAM and (iii) CoTCAPc modified gold electrode. The decrease in R_{CT} on the CoTCAPc SAM modified electrode is attributed to the facilitation of electron transfer and also it can be attributed to the permeability of SAM to the solution ions due to its functional groups, i.e. −OH for Au-ME SAM and −COOH for Au-ME-CoTCAPc SAM. Thus, coordination of CoTCAClPc to Au-ME SAM resulted in structural change of the Au-ME SAM, hence surface properties, resulting in the observed differences in Warburg line. The increase in R_{CT} upon immobilizing with the enzyme is attributed to the surface being blocked by the enzyme. These impedance measurements are found to be consistent with the cyclic voltammograms obtained in Fig. 1.

3.4. Electrocatalysis and amperometric detection of H_2O_2 at Au-ME-CoTCAPc SAM

Fig. 3(a) shows the cyclic voltammograms of Au-ME-CoTCAPc SAM in PBS (pH 7.4) solution without hydrogen peroxide and with 0.1 mM hydrogen peroxide, Fig. 3(b). An irreversible peak which corresponds to Co^{II}TCAPc/Co^{I}TCAPc, was observed at −200 mV in Fig. 3(a) [30]. In the presence of H_2O_2, Fig. 3(b) shows the electrocatalytic oxidation and the reduction of H_2O_2 at 600 and −200 mV, respectively. It is interesting to note that at the bare gold electrode within the studied potential, Fig. 3 (insert) no peaks due oxidation or reduction of H_2O_2 were observed. From the CVs (bare and modified electrode) it is discernible that Au-ME-CoTCAPc

SAM mediates the oxidation and the reduction of H_2O_2. The possible mechanisms for these observations are summarized in Eqs. (2), (3), (4) and (5):

$$Co^{II}Pc \rightarrow Co^{III}Pc + e^- \quad (2)$$

$$Co^{III}Pc + \tfrac{1}{2}H_2O_2 \rightarrow \tfrac{1}{2}O_2 + H^+ + Co^{II}Pc \quad (3)$$

$$Co^{II}Pc + e^- \rightarrow Co^{I}Pc \quad (4)$$

$$Co^{I}Pc + \tfrac{1}{2}H_2O_2 + H^+ \rightarrow H_2O + Co^{II}Pc \quad (5)$$

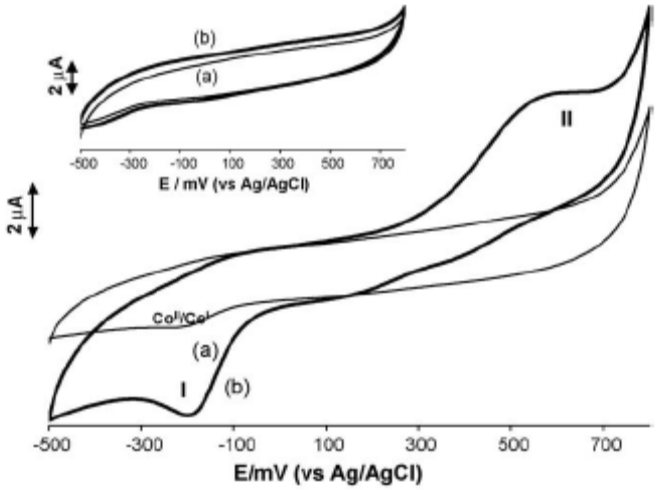

Fig. 3. Cyclic voltammograms of Au-ME-CoTCAPc SAM (a) without H_2O_2, and (b) with 1×10^{-4} M H_2O_2 in 0.01 M PBS (pH 7.4) solution. Inset cyclic voltammograms of bare gold electrode (a) without H_2O_2, and (b) with 1×10^{-4} M H_2O_2 in 0.01 M PBS (pH 7.4) solution. (Scan rate = 25 mV/s).

It is clear in Fig. 3(b) that on addition of H_2O_2, there is an enhancement of currents in the region of Co^{II}/Co^{I} hence this couple catalyses H_2O_2 reduction, with a peak labeled I. H_2O_2 oxidation (peak II) is catalyzed by Co^{III}/Co^{II} since the peak is at the range for this couple. Based on these observations, Eqs. (2) and (3) correspond to the H_2O_2 oxidation and Eqs. (4) and (5) correspond to the H_2O_2 reduction. Eqs. (2) and (3) are known mechanistic steps for the oxidation of H_2O_2 at CoPc modified electrode [2] and [12]. First the metal oxidation takes place from Co^{II}TCAPc to Co^{III}TCAPc (Eq. (2)), followed by oxidation of H_2O_2 to molecular oxygen as the metal is reduced back to Co^{II}TCAPc (Eq. (3)). Eqs. (4) and (5) are proposed mechanistic steps for the reduction of H_2O_2 at CoPc modified electrode. The metal reduction takes place from Co^{II}TCAPc to Co^{I}TCAPc (Eq. (4)), followed by the reduction of H_2O_2 to water as the metal is oxidized from Co^{I}TCAPc to Co^{II}TCAPc (Eq. (5)). The oxidation of H_2O_2 at CoPc modified electrode is known [2] and [12], however the reduction of H_2O_2 has only been done at enzyme electrode [16] and to our knowledge no report of H_2O_2 reduction at CoPc modified electrode. Therefore, the proposed reduction mechanism for H_2O_2 was further investigated using spectroscopic methods whereby first the generation of Co^{I}TCAPc from Co^{II}TCAPc was achieved by using a strong reducing agent, $NaBH_4$. Fig. 4A is a typical spectrum showing the generation of Co^{I}TCAPc

upon adding $NaBH_4$ in DMF solution of $Co^{II}TCAPc$. The Q-band at 676 nm decreased in intensity while new bands at 710 and 480 nm appear as the reduction process continues, Fig. 4A(b). These changes are known for the reduction of CoPc, the absorption band at 480 nm is typical of $Co^{I}TCAPc$ species [51]. Following the formation of $Co^{I}TCAPc$ species, addition of H_2O_2 resulted in the oxidation of $Co^{I}TCAPc$ back to $Co^{II}TCAPc$ (Fig. 4B(b)) as evidenced by the decrease in bands at 480 and 710 nm. The spectra of the regenerated $Co^{II}TCAPc$ did not completely go back to the original in Fig. 4A(a), which consisted mainly of the monomer, but showed aggregation when left to react with H_2O_2 over long periods as shown by the typical dimer peak at 638 nm, Fig. 4B(c). These spectral changes proved the regeneration of $Co^{II}TCAPc$ in the presence of H_2O_2 even though aggregated.

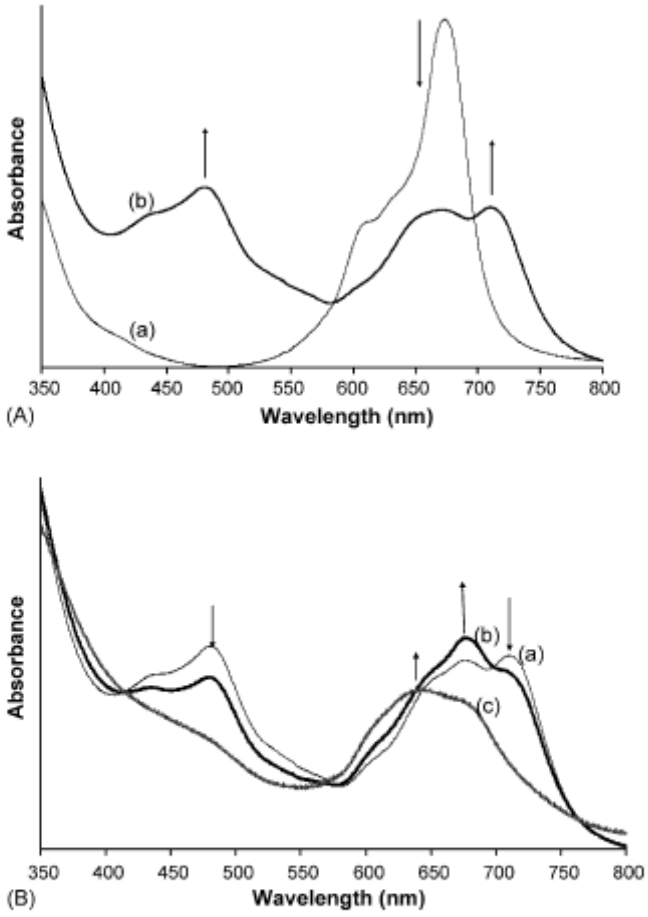

Fig. 4. (A) UV–vis spectral changes observed during the reduction of $Co^{II}TCAPc$ to $Co^{I}TCAPc$ (a) before adding $NaBH_4$ and (b) after adding $NaBH_4$ an oxidizing agent in DMF. (B) UV–vis spectral changes observed during the oxidation of $Co^{I}TCAPc$ to $Co^{II}TCAPc$ (a) before adding H_2O_2, (b) after adding H_2O_2 an oxidizing agent in DMF, and (c) spectrum of H_2O_2 recorded in a long period. The first trace (b) in Fig. 3B is the same as the last trace in Fig. 3A(a).

Fig. 5A shows the typical chronoamperomogram of Au-ME-CoTCAPc SAM upon consecutive additions of H_2O_2 at a fixed oxidative potential (600 mV). The response of Au-ME-CoTCAPc SAM modified gold electrode was investigated under stirring in PBS (pH 7.4) solution with 0.5 μM H_2O_2 added in steps. A base line was established in 10 mL of PBS (pH 7.4) solution. A well-defined current response due to H_2O_2 oxidation was observed with successive increments of H_2O_2 concentration in solution (indicated by arrows). However, the successive addition of 0.5 μM H_2O_2 led to the

decrease in current response, signifying saturation in concentration. Fig. 5A (inset) displays the calibration curve (the plot of current response versus concentration of H_2O_2) for the Au-ME-CoTCAPc, which yielded a straight line within the studied concentration range (0.5–5 μM) with the correlation coefficient of 0.993. The limit of detection (LoD) was found to be 0.4 μM at 3σ and the electrode gave the best response time of approximately 1 s to the additions of H_2O_2. This electrode gave the best results towards the electrocatalytic oxidation H_2O_2 than the recent reports which found 8.0 μM for the detection of H_2O_2 using carbon paste electrodes modified with nanostructured cryptomelane-type manganese oxides [11], glassy carbon electrode modified with CoPc-$(CoTPP)_4$ using a drop dry method [15] and horseradish peroxidase-colloid gold-based sensor [16], but performed less satisfactorily compared to when glassy carbon electrode combined with carbon nanotube (CNT) and nano-platinum (nano-Pt) was employed [52].

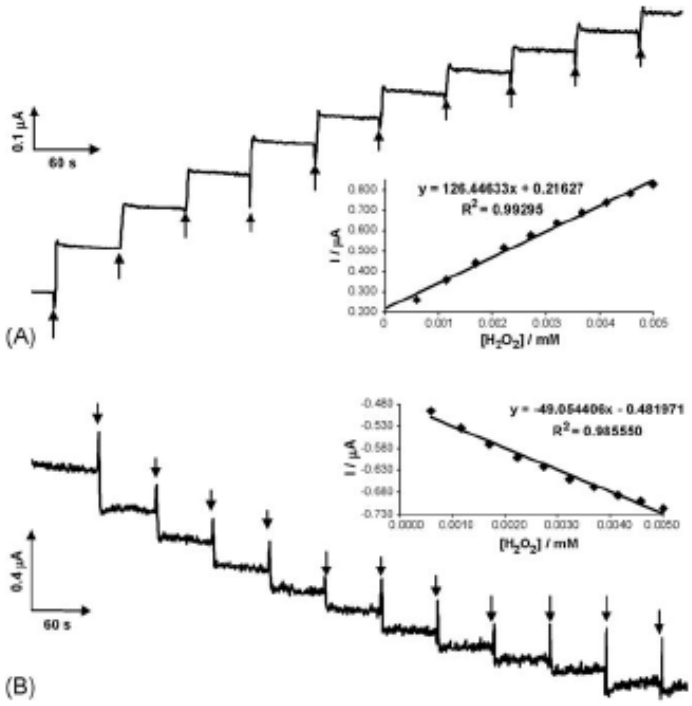

Fig. 5. (A) Amperometric current response of Au-ME-CoTCAPc SAM on additions (indicated by arrows) of 1×10^{-4}M H_2O_2 in 0.01 M PBS solutions at 600 mV applied potential. Inset, is the linear plot of current vs. concentration of H_2O_2. (B) Amperometric current response of Au-ME-CoTCAPc SAM on additions (indicated by arrows) of 1×10^{-4} M H_2O_2 in 0.01 M PBS solutions at −200 mV applied potential. Inset, is the linear plot of current vs. concentration of H_2O_2.

Fig. 5B shows a typical chronoamperomogram of Au-ME-CoTCAPc SAM upon successive additions of H_2O_2 at applied reduction potential (−200 mV). The similar procedure used above for the oxidation of H_2O_2 was employed, except that the applied potential was −200 mV. The negative increase in current response due to the reduction of H_2O_2 was observed with successive increments of 0.5 μM H_2O_2 concentration in solution (indicated by arrows). In the same way as the oxidation, the successive increase in concentration of H_2O_2 led to a decrease in the current response as a result of saturation in concentration. Fig. 5B (inset) displays the calibration curve of Au-ME-CoTCAPc electrode which gave a linear plot within the studied concentration range 0.5–5 μM with a coefficient of 0.986. The LoD was found to be 0.2 μM at 3σ and the electrode gave the best response time of approximately 1 s.

Compared to 8.0 μM obtained from the horseradish peroxidase-colloid gold-based sensor [16] this electrode gave the best response time (~1 s) and best LoD (0.2 μM). Since the general mechanism for the glucose oxidase (GOx)-based amperometric sensing involves the use of MPc as an electron mediator (Scheme 1), the immobilized enzyme (GOx) was then studied for glucose analysis.

3.5. Amperometric response of glucose at Au-ME-CoTCAPc-GOx SAM

The oxidation potential of 600 mV (also used for H_2O_2 above) was chosen as the working potential for the detection of glucose on Au-ME-CoTCAPc-GOx SAM. Fig. 6A shows the plot of the current response of the Au-ME-CoTCAPc-GOx SAM electrode as a function of glucose concentration, i.e. the plot of steady-state current (I_{ss}) versus glucose concentration (C). Fig. 6A (insert) shows a typical chronoamperomogram of Au-ME-CoTCAPc-Gox SAM upon successive additions of 0.3 mM glucose. The calibration curve is linear for the concentration range 0.3–25 mM and then curvature at higher concentration was observed. This linear concentration range of 0.3–25 mM is of advantage as is almost within the likely glucose level in normal and diabetic person which is (0.2–20 mM) [53]. In comparison with the values reported in Table 1, this enzyme electrode gave a wider linear concentration range of up to 25 mM than the other CoPc-enzyme modified electrodes. The enzyme electrode (Au-ME-CoTCAPc-GOx SAM) exhibited a rapid response (1 s) to the changes of glucose concentrations indicating excellent electrocatalytic behavior of this biosensor electrode. The LoD at 3σ was found to be 8.4 μM and this value was found to be almost similar to the value obtained using a nanogold particle by Zhang et al. [54] and was slightly higher than other CoPc electrodes in Table 1. The sensitivity of the biosensor which is 7.5 nA/mM was obtained from the slope of the linear part of the calibration curve (Fig. 6A).

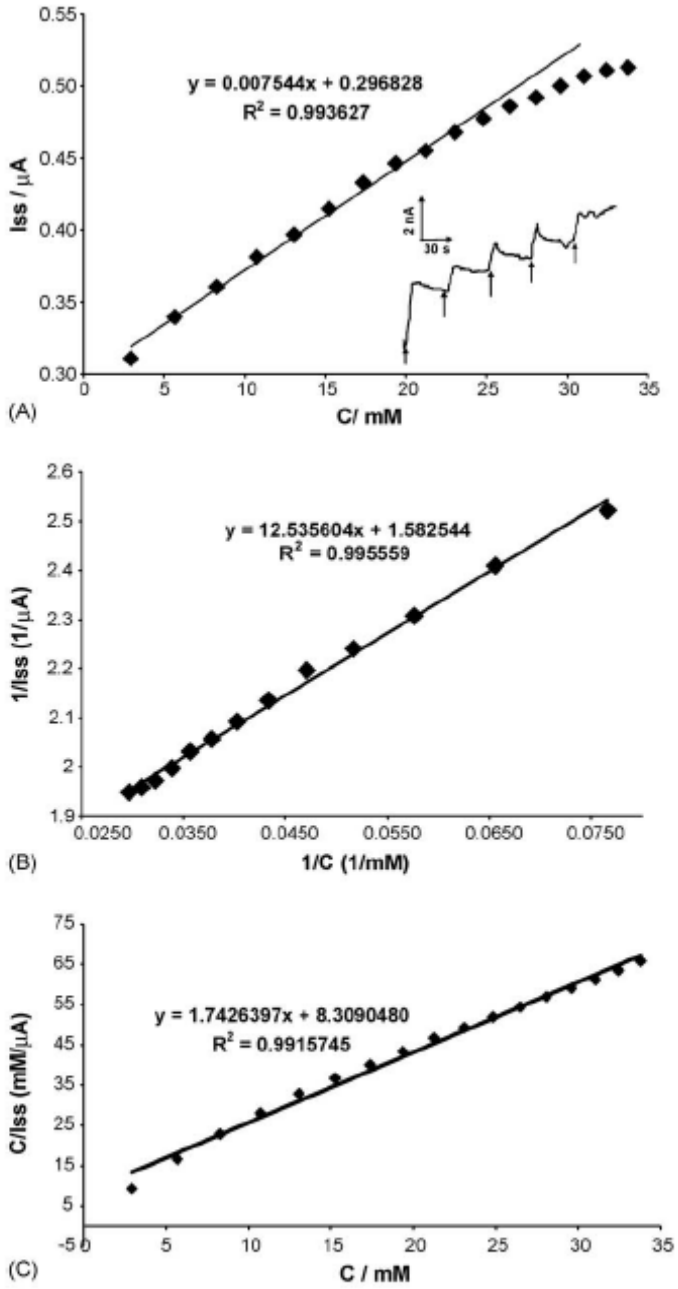

Fig. 6. (A) Calibration curve of current response of Au-ME-CoTCAPc-GOx SAM vs. glucose concentration in PBS (pH 7.4) solution at applied potential 600 mV. Inset amperometric current response of Au-ME-CoTCAPc-GOx SAM on additions (indicated by arrows) of 0.1 M Glucose in 0.01 m PBS solution at 600 mV applied potential. (B) Lineweaver–Burk plot of $1/I_{ss}$ vs. $1/C$ according to data in (A). (C) Hanes plot of C/I_{ss} vs. C according to data in (A).

Table 1
Kinetic data for the different electrode modifiers as mediators at electrodes surfaces for glucose oxidase (GOx)-based enzyme sensors, compared to the one reported in this work

Modifier	Method	LCR (mM)	LoD	K_m^{app} (mM)	Response time (s)	Sensitivity	i_{max} ($\mu A\,cm^{-2}$)	Ref.
CoTCAPc	Au-ME-CoTCAPc-GOx	0.1–25	8.4 μM	7.9 4.8	1	7.5 nA/mM	31.4 28.6	This work
$(OEt)_8$CoPc	CPM-$(OEt)_8$CoPc-GOx	≤4	3 μM	–	<5	–	–	[26]
CoPc	CPM-CoPc-GOx	≤4	3 μM	–	<5	–	–	[26]
OsPVP	Au-MPS-OsPVP-GOx	0.1–10	50 μM	8.5	10	–	–	[23]
CoTAPc	GCE-CoTAPc-GOx-Naf	0.001–5	0.5 μM	–	–	–	–	[2]
CoPc	SPCE-CoPc-GOx	0.2–5	0.2 μM	–	–	$1.12\,\mu A\,mM^{-1}$	–	[28]
Nano-CoPc	PGE-nano-CoPc-GOx	0.02–18	5 μM	12.4	5	$7.7\,mA\,mM^{-1}\,cm^{-2}$	–	[17]

Abbreviations: LCR, linear concentration range; LoD, limit of detection; K_m^{app}, Michaelis-Menten constant; i_{max}, maximum current; CoTCAPc, cobalt tetracarboxylic acid phthalocyanine; 2-ME, 2-mercaptoethanol; GOx, glucose oxidase enzyme; $(OEt)_8$CoPc, octaethoxy cobalt phthalocyanine; CPM, carbon paste matrix; CoPc, cobalt phthalocyanine; OsPVP, Osmium poly-(4-vinyl)pyridine; MPS, (3-mercaptopropyl)trimethoxysaline; CoTAPc, cobalt tetraamino phthalocyanine; Naf., nafion membrane; GCE, glassy carbon electrode; nano-CoPc, nano cobalt phthalocyanine; PGE, poly graphite electrode.

At high glucose concentrations (above 25 mM) a current plateau can be observed, in Fig. 6A. The curvature from the initial straight line shows the characteristics of Michaelis–Menten kinetics. The apparent Michaelis–Menten constant (K_m^{app}), which gives an indication of the enzyme-substrate kinetics for the biosensor (Au-ME-CoTCAPc-GOx SAM) electrode can be calculated from an electrochemical version of Lineweaver–Burk [55] and Hanes [56] equation. Many reports are based on Lineweaver–Burk, hence both are discussed in this work. The Lineweaver–Burk Eq. (6) follows:

$$\frac{1}{I_{ss}} = \frac{K_m^{app}}{i_{max}}\frac{1}{C} + \frac{1}{i_{max}} \tag{6}$$

where I_{ss} is the steady-state current after the addition of the substrate, i_{max} the maximum current measured under substrate saturation condition, and C is the concentration of the substrate. The K_m^{app} value was calculated from the slope (K_m^{app}/i_{max}) and the intercept ($1/i_{max}$) from the plot of reciprocal steady-state current versus the reciprocal of glucose concentration (Fig. 6B). The K_m^{app} value for the Au-ME-CoTCAPc-Gox SAM was found to be 7.9 mM, which is smaller than the recently reported value for nano-CoPc [17], in Table 1. The smaller K_m^{app} value means that the immobilized enzyme (GOx) possesses a higher enzyme activity and the proposed electrode exhibits a higher affinity for glucose. The data was also analyzed using the plot of C/I_{ss} versus C (referred to as Hanes plot) from the Eq. (7):

$$\frac{C}{I_{ss}} = \frac{C}{i_{max}} + \frac{K_m^{app}}{i_{max}} \tag{7}$$

the symbols are the same as defined in Lineweaver–Burk equation, above. The K_m^{app} value was determined by analysis of the slope ($1/i_{max}$) and the intercept (K_m^{app}/i_{max}), Fig. 6C. The K_m^{app} value of the biosensor (Au-ME-CoTCAPc-GOx SAM) electrode was found to be 4.8 mM, noticeably smaller than 7.9 mM calculated using Lineweaver–Burk equation. According to Cornish-Bowden [56] the Lineweaver–Burk plot gives a grossly misleading impression of experimental errors hence over-estimates K_m^{app} values, compared to Hanes plot which gives fair range of errors leading to realistic K_m^{app} values. These results imply that the biosensor (Au-ME-CoTCAPc-GOx SAM) electrode with CoTCAPc as a mediator on gold electrode is actually valuable and sensitive. The long-term stability of the enzyme was studied by recording the current response of the enzyme upon addition of glucose under stirring conditions. We noticed that after four successive days, 76% of the current response was retained and this current response dropped drastically after that the fifth day to about 36%. This may be due to the loss of enzyme activity.

3.6. Possible application real sample and interference studies

The applicability of the developed biosensor electrode towards real sample detection was assessed with a commercially available clinical ALPHA® glucose powder chronoamperometrically. From standard addition method, the glucose content was 99.97. ± 0.06% (n = 7). The result is in conformity with the expected clinical glucose content and manufacturers' values. These results indicate the suitability of the developed biosensor (Au-ME-CoTCAPc-GOx SAM) towards a quick clinical analysis of glucose solution.

An important analytical parameter for a biosensor is its ability to discriminate between the interfering species commonly present in similar physiological environment and the target analyte. The effect of the common electroactive interferents such as cysteine, ascorbic acid, oxalic acid and uric acid to the response of glucose with Au-ME-CoTCAPc-GOx SAM was investigated using the mixed solution method [57]. These interferent species were selected as they are likely to appear in biological and food samples. The concentration of these interfering species was chosen as the concentration close to their relevant clinical levels [58], i.e. in the orders of 10^{-4} M while that of the glucose was maintained at 10^{-3} M. The values of K_{amp} (where K_{amp} is the amperometric selectivity coefficient) were determined from Eq. (8) reported in literature [56] for the analysis in the presence of the interference species:

$$K_{amp} = \left(\frac{\Delta I_{mixture}}{\Delta I_{glucose}} - 1\right) \times \left[\frac{\text{glucose}}{\text{interference} - \text{species}}\right] \quad (8)$$

where $\Delta I_{mixture}$ and $\Delta I_{glucose}$ are, respectively, the changes in current for the mixture containing glucose and interfering ions, and glucose alone. The estimated K_{amp} values for the interference species are: cysteine ($\sim 8 \times 10^{-3}$), ascorbic acid (0.0186), oxalic acid (6.36×10^{-5}) and uric acid (8.97×10^{-3}). The K_{amp} value less than 10^{-3} (as for oxalic acid) indicates a non-interfering species and the K_{amp} values greater than 10^{-3} (as for ascorbic acid) indicates an interfering species [57]. However, if the K_{amp} values fall within orders of 10^{-3} (as for L-Cysteine and uric acid), they indicate that the species is an interferent but not a strong one. These K_{amp} values thus suggest that ascorbic acid is a strong interferent while the other species (uric acid, L-cysteine and oxalic acid) are relatively not interfering with glucose detection. Therefore, the electrode can be successfully used for the detection of glucose in the presence of cysteine, oxalic acid and uric acid under the conditions employed in this work.

4. Conclusion

In conclusion, this report describes the Au-ME-CoTCAPc SAM as an efficient amperometric sensor for hydrogen peroxide at physiological pH conditions. The reduction mechanism for H_2O_2 has been shown to involve Co^{II}/Co^{I} while the oxidation mechanism involves Co^{III}/Co^{II}. The Au-ME-CoTCAPc SAM sensor exhibited good results as an amperometric sensor with good detection limits: 0.4 μM oxidatively and 0.2 μM reductively. The sensor also gave good response time ($\sim$1 s) with good linearity up to 5 μM for both oxidation and reduction. We also further investigated the fabrication of the glucose oxidase enzyme covalently attached to CoTCAPc on gold electrode as a biosensor for glucose with Au-Me-CoTCAPc SAM which acted as an electron mediator. The biosensor showed good activity towards the detection of glucose with the low Michaelis–Menten constant (4.8 mM, from Hanes plot) and wide linear concentration range (0.3–25 mM), making this biosensor a viable glucose biosensor.

Acknowledgements

This work was supported by the National Research Foundation, (GUN 2069275 and GUN 2053657), Rhodes University. P.M. would like to thank Project AuTEK (Mintek and GoldFields) for financial support. K.I.O. thanks the Mellon Foundation program for an accelerated development.

References

[1] C. Matsubara, N. Kawamoto and K. Takamura, *Analyst* 117 (1992), p. 1781

[2] G. Shi, J. Lu, F. Xu, H.G. Zhou, L. Jin and J. Jin, *Anal. Chim. Acta* 314 (2000), p. 131.

[3] U. Pinkernell, S. Effkemann and U. Karst, *Anal. Chem.* 69 (1997), p. 3623.

[4] N. Kiba, T. Tokizawa, S. Kato, M. Tachibana, K. Tani, H. Koizumi, M. Edo and E. Yonezawa, *Anal. Sci.* 19 (2003), p. 823.

[5] M.J. Navas, A.M. Jiménez and G. Galán, *Atmos. Environ.* 33 (1999), p. 2279.

[6] E.C. Hurdis and H. Romeyn Jr, *Anal. Chem.* 26 (1954), p. 320

[7] E. Ferapontova and L. Gorton, *Bioelectrochemistry* 55 (2002), p. 83.

[8] E.E. Ferapontova, V.G. Grigorenko, A.M. Egorov, T. Bőrchers, T. Ruzgas and L. Gorton, *Biosens. Bioelectron.* 16 (2001), p. 147.

[9] E. Ferapontova, K. Schmengler, T. Bőrchers, T. Ruzgas and L. Gorton, *Biosens. Bioelectron.* 17 (2002), p. 953.

[10] A. Morales, F. Céspedes, J. Muňoz, A. Martinez-Fasbregas and S. Alegret, *Anal. Chim. Acta* 332 (1996), p. 131.

[11] Y. Lin, X. Ciu and L. Li, *Electrochem. Comm.* 7 (2005), p. 166.

[12] M.A. Gilmartin, R.J. Ewen and J.P. Hart, *J. Electroanal. Chem.* 401 (1996), p. 127.

[13] M.S.M. Quintino, H. Wimischofer, K. Araki, H.E. Toma and L. Angnes, *Analyst* 130 (2005), p. 221.

[14] M. Somasundrum, K. Kirtikara and M. Tanticharoen, *Anal. Chim. Acta* 319 (1996), p. 59.

[15] K.I. Ozoemena, Z. Zhao and T. Nyokong, *Electrochem. Comm.* 7 (2005), p. 679.

[16] L. Wang and E. Wang, *Electrochem. Comm.* 6 (2004), p. 225.

[17] K. Wang, J.J. Xu and H.Y. Chen, *Biosens. Bioelectron.* 20 (2005), p. 1388.

[18] M.A. Gilmartin, R.J. Ewen, J.P. Hart and C.L. Honeybourne, *Electroanalysis* 7 (1995), p. 547.

[19] A. Bettelheim, D. Ozer, R. Harth and R. Ydgar, *J. Electrochem. Chem.* 281 (1990), p. 147.

[20] S. Warren, T. McCormac and E. Dempsey, *Bioelectrochemistry* 67 (2003), p. 23.

[21] D. Pan, J. Chen, L. Nie, W. Tao and S. Yao, *Electrochim. Acta* 49 (2004), p. 795.

[22] J. Fei, Y. Wu, X. Ji, J. Wang, S. Hu and Z. Gao, *Anal. Sci.* 19 (2003), p. 1259.

[23] S.-F. Hou, K.-S. Yang, H.-Q. Fang and H.-Y. Chen, *Talanta* 47 (1998), p. 561.

[24] M.E. Ghica and C.A. Brett, *Anal. Chim. Acta* 532 (2005), p. 145.

[25] I. Rosen-Margalit, A. Bettelheim and J. Rishpon, *Anal. Chim. Acta* 281 (1993), p. 327.

[26] F. Mizutani, S. Yabuki and S. Iijima, *Anal. Chim. Acta* 300 (1995), p. 59.

[27] J.P. Hart and S.A. Wring, *TrAC* 16 (1997), p. 89.

[28] E. Crouch, D.C. Cowell, S. Hoskins, R.W. Pittson and J.P. Hart, *Anal. Biochem.* 347 (2005), p. 17

[29] X. Zhong, R. Yuan, Y. Chai, Y. Liu, J. Dai and D. Tang, *Sens. Actuators B* 104 (2005), p. 191.

[30] P.N. Mashazi, K.I. Ozoemena, D.M. Maree and T. Nyokong, *Electrochim. Acta* 52 (2006), p. 3489

[31] D. Song, Y. Mu, X. Liu, L. Zhao, H. Zhang and Q. Jin, *Microchem. J.* 74 (2003), p. 93.

[32] D.L. Pilloud, X. Chen, P.L. Dutton and C.C. Mosser, *J. Phys. Chem. B* 104 (2000), p. 2868.

[33] D. Losic, J.G. Shapter and J.J. Gooding, *Langmuir* 17 (2001), p. 3307.

[34] J.J. Gooding, L. Pugliano, D.B. Hibbert and P. Erokhin, *Electrochem. Comm.* 2 (2000), p. 217.

[35] J.J. Gooding and D.B. Hibbert, *TrAC* 18 (1999), p. 525.

[36] J.J. Gooding, P. Erokhin and D.B. Hibbert, *Biosens. Bioelectron.* 15 (2000), p. 229.

[37] L. Jiang, A. Glidle, A. Griffith, C.J. McNeil and J.M. Cooper, *Bioelectrochem. Bioenerg.* 42 (1997), p. 15.

[38] S.E. Creager, L.A. Hockett and G.K. Rowe, *Langmuir* 8 (1992), p. 854.

[39] H.O. Finklea In: A.J. Bard and L.R. Rubinstein, Editors, *Electrochemistry of Organized Monolayers of Thiols and Related Molecules on Electrodes*, *Electroanalytical Chemistry* vol. 19, Marcel Dekker, New York (1996), p. 109.

[40] U. Oesch and J. Janata, *Electrochim. Acta* 28 (1983), p. 1237.

[41] K.V. Gobi, T. Okajima, K. Tokuda and T. Ohsaka, *Langmuir* 14 (1998), p. 1108.

[42] Z. Wang, A.-M. Nygard, M.J. Cook and D.A. Russell, *Langmuir* 20 (2004), p. 5850.

[43] J.-S. Ye, Y. Wen, W.D. Zhang, H.F. Cui, G.Q. Xu and F.-S. Shen, *Electroanalysis* 17 (2005), p. 89.

[44] P. Ocon, P. Herrasti, L. Vazquez, R.C. Salvarezza, J.M. Vara and A.J. Avria, *J. Electroanal. Chem.* 319 (1991), p. 101.

[45] S.-S. Wong and M.D. Porter, *J. Electroanal. Chem.* 485 (2000), p. 135.

[46] Z. Li, M. Lieberman and W. Hill, *Langmuir* 17 (2001), p. 4887.

[47] Y.-H. Tse, P. Janda, H. Lam, J. Zhang, W.J. Pietro and A.B.P. Lever, *J. Porph. Phthal.* 1 (1997), p. 3.

[48] M.D. Porter, T.B. Bright, D.L. Allara and C.D.E. Chidsey, *J. Am. Chem. Soc.* 109 (1987), p. 3559.

[49] A. Lasia and A. Rami, *J. Electroanal. Chem.* 294 (1990), p. 123.

[50] C. Amatore, J.M. Saveant and D. Tessier, *J. Electroanal. Chem.* 147 (1983), p. 39.

[51] M.J. Stillman and T. Nyokong In: C.C. Leznoff and A.B.P. Lever, Editors, *Phthalocyanines: Properties and Applications* vol. 1, VCH Publishers, New York (1989).

[52] S. Hrapovic, Y. Liu, K.B. Male and J.H.T. Luong, *Anal. Chem.* 76 (2004), p. 1083.

[53] B.R. Eggins, Chemical Sensors and Biosensors, John Wiley & Sons, UK (2003) p. 111.

[54] S. Zhang, N. Wang, H. Yu and C. Sun, *Bioelectronics* 67 (2005), p. 15.

[55] R.A. Kamin and G.S. Wilson, *Anal. Chem.* 52 (1980), p. 1198. [56] A. Cornish-Bowden, Fundamentals of Enzyme Kinetics, Butterworths, London (1979) p. 17.

[57] R.I. Stefan, J.F. van Staden and H.Y. Aboul-Enien, Electrochemical Sensors in Bioanalysis, Marcel Dekker, New York (2001) p. 65.

[58] H. Zhou, H. Chen, S. Luo, J. Chen, W. Wei and Y. Kuang, *Sens. Actuators B* 101 (2004), p. 224.